Energy Balance Simulation for Surface Soil and Residue Temperatures with Incomplete Cover

Robert M. Aiken, Gerald N. Flerchinger, Hamid J. Farahani, and Karen E. Johnsen

Reprinted from *Agronomy Journal*
Vol. 89, No. 3

Energy Balance Simulation for Surface Soil and Residue Temperatures with Incomplete Cover

Robert M. Aiken,* Gerald N. Flerchinger, Hamid J. Farahani, and Karen E. Johnsen

ABSTRACT

Knowledge of the effects that crop residue architecture has on exchange processes at the soil surface can extend the applicability of soil and water balance modules. Our objectives were to evaluate the feasibility of using a numerically reduced soil–residue energy boundary condition module, compatible with the USDA-ARS Root Zone Water Quality Model, and to compare the accuracy of calculated values against measurements. We developed a Penman-type energy balance module, PENFLUX, which solves for surface temperatures of a soil slab and a single flat residue layer, adjusting for aerodynamic resistances of standing residue stems. It provides surface boundary conditions for simulations of energy transfer in a one-dimensional soil profile. PENFLUX simplifies iterative solutions by simplifying radiation, convection, and soil heat algorithms. We collected hourly radiation data; air, soil, and residue temperatures; and wind profile data after wheat harvest on a level Nunn clay loam soil (fine, smectitic, mesic Aridic Argiustoll) (1997 soil series reclassification). Model parameterization avoided fitting model calculations to measurements, as inputs were measured at the site or referenced from literature. PENFLUX calculations exhibited a low degree of random error for dry soil and residue conditions, though systematic bias in surface soil temperature and negative bias in nighttime net irradiance reduced predictive efficiency. Error propagated from surface soil temperature probably contributes to the negative bias in net radiation. The reasonable predictive accuracy of PENFLUX for dry soil conditions demonstrates the feasibility of a numerically simplified model of soil–residue energy exchanges, and justifies further evaluation against a range of residue architectures and environmental conditions.

LAND MANAGEMENT can be enhanced by accurate simulation of energy exchange processes in the soil–residue–atmosphere system. Emergence and development of crops, their pests, and various soil organisms are altered by heat and water movement near the soil–atmosphere interface. Accurate simulation of heat and water transport in soil can complement remote sensing techniques for monitoring surface soil water distribution (Lascano and Van Bavel, 1983). Knowledge of plant residue effects on the soil energy balance can guide farm and regional assessment of residue management alternatives for soil, water, and nutrient conservation; pest management; and plant development processes (Van Doren and Allmaras, 1978).

Residue management affects the thermal dynamics of evaporative surfaces. Residue architecture (dimension, frequency, and orientation of residue elements) modifies radiative and advective exchange processes between soil and atmosphere (Lyles and Allison, 1976; Ross et al., 1985; Raupach, 1992). Bristow and Abrecht (1989) showed that strips of partial mulch cover improved preplant soil warming by increasing absorption and retention of solar irradiance. Increased soil water storage was attributed to greater snow catch with vertical rather than horizontal residue orientation (Nielsen and Hinkle, 1994), and to improved infiltration and reduced evaporation with higher quantities of residue loading (Doran et al., 1984). Surface residues can increase the crop water use efficiency by increasing the transpiration component of total evaporation (Lascano et al., 1994). Robust simulations, providing accurate calculations of energy exchange processes from weather driving variables and readily measured soil and residue properties, can guide field experiments designed to test critical hypotheses distinguishing residue and tillage effects on soil thermal and hydric regimes.

Incomplete knowledge of soil surface temperature and heat flux boundary conditions frequently constrains the solution of soil heat and water balance modules (RZWQM Team, 1992). Empiricisms relating surface and ambient temperatures can quantify seasonal residue effects at a regional scale (Gupta et al., 1984), but provide limited insight to exchange processes. Process-level algorithms quantify soil–atmosphere energy exchanges under a range of residue architectures, but require extended numerical solutions or neglect significant exchange processes.

Integrated, process-level numerical models of energy exchange in the soil–residue–atmosphere system enhance our understanding of environmental factors driving heat and vapor transport. The conceptual models of Hillel et al. (1975) and Chung and Horton (1987) treat residues and mulches as opaque and hydrophobic obstructions to radiative and convective transport processes. Mahrer (1979) expanded these concepts to allow for soil–residue exchange processes, including transmission of shortwave irradiance with incomplete residue cover, longwave radiative exchange and diffusion of sensible heat. Sui et al. (1992), Lascano et al. (1994), and Grant et al. (1995) derived similar models and evaluated simulated values with field measurements. Ross et al. (1985) advanced process-level simulation by applying the radiative transfer theory of Norman and Jarvis (1975) to residue architectures. Bristow et al. (1986) provided for forced convective exchanges among residue elements, the adjacent air, and the soil surface, while also simulating water interception, storage, and evaporation in the flat residue sublayer. Hares and Novak (1992) and Bussiere and Cellier (1994) derived simi-

R.M. Aiken, H.J. Farahani, and K.E. Johnsen, USDA-ARS Great Plains Systems Res., P.O. Box E, Fort Collins, CO 80522; G.N. Flerchinger, USDA-ARS Northwest Watershed Res. Ctr., 800 Park Blvd., Plaza IV, Suite 105, Boise, ID 83712. Received 4 Mar. 1996. *Corresponding author (aiken@gpsr.colostate.edu).

Published in Agron. J. 89:404–415 (1997).

lar soil–residue models, which were also evaluated with field measurements.

This literature reflects an emerging theory of near-surface energy exchange under canopies of plant residues. However, the applicability of this theory to landscape analysis and decision support is limited either by the extended numerical requirements of integrated soil–residue simulations, or by analytic solutions that neglect significant exchange processes. Robust models of surface boundary conditions, models that maintain accurate energy balance closure with limited knowledge of soil state and system parameters, are well developed in the case of soil–canopy systems (Shuttleworth and Wallace, 1985; Choudhury and Monteith, 1988; Luo et al., 1992). Stannard (1993) found that the dual-source evaporation model of Shuttleworth and Wallace (1985) quantified hourly potential evapotranspiration with negligible bias and moderate accuracy (r^2 = 0.78) for soil–canopy systems. Luo et al. (1992) developed an analytic energy balance module that quantified thermal gradients within soil–canopy systems; this module provided upper boundary conditions for soil water and temperature modules simulating energy and water exchange in the soil–canopy–atmosphere system. Analogous surface boundary condition models quantifying residue effects on surface boundary conditions are incompletely developed. Grant et al. (1995) presented a surface boundary condition solution to the soil energy balance for an opaque residue layer with variable soil cover, but neglected soil–residue convective and radiative exchange processes that can shift partitioning of energy balance components.

Our objective was to evaluate the feasibility of using a numerically simplified, yet physically based model of soil–residue–atmosphere energy exchange as a surface boundary condition for soil heat and water balance modules of the Root Zone Water Quality Model (RZWQM Team, 1992). The boundary condition solution combines a set of Penman-type energy balance equations with a truncated soil heat flux algorithm under a residue sublayer. (This is hereafter referred to as the PENFLUX module.) We compare the calculated values of the boundary condition solution with field measurements of net irradiance and temperatures of flat residue elements and the surface soil, obtained after wheat harvest.

MATERIALS AND METHODS

Simulation

Soil energy transfer processes were simulated using soil heat modules of a Simultaneous Heat and Water Model (SHAW) (Flerchinger and Saxton, 1989) implemented within the Root Zone Water Quality Model (RZWQM Team, 1992), hereafter referred to as RZ_SHAW. The soil heat modules of RZ_SHAW use a Newton–Raphson convergence scheme that solves finite difference expressions of the energy balance equations for soil temperature profiles. Water flux densities, required by RZ_SHAW soil heat modules to compute heat convection by water transport, are provided by soil water balance modules of RZWQM, which include a modified Green–Ampt approach to infiltration and a finite-difference formulation of Richard's equation for water redistribution. Surface boundary conditions required by the RZ_SHAW soil heat modules for solution of soil temperature profiles are provided by PENFLUX, a soil–residue energy balance module, using the Penman transformation, formulated for a soil slab under incomplete residue cover.

Soil Energy Balance

Heat flow in a nonfreezing soil, neglecting horizontal gradients, is described by a one-dimensional convection–diffusion equation

$$C_s \frac{\partial T_z}{\partial t} + \left(\frac{\theta_a \lambda M_w}{R T_{zK}}\right) \frac{\partial e_s}{\partial t} = \frac{\partial}{\partial z}\left[k_{t(s)} \frac{\partial T_z}{\partial z}\right] - C_w q_w \frac{\partial T_z}{\partial z} + \lambda \frac{\partial q_v}{\partial z} \quad [1]$$

which is subject to upper and lower boundary conditions. Definitions of variables are provided in the Appendix, along with their SI units. The lower boundary condition is held constant at a user-defined temperature. Terms on the left-hand side represent change in energy stored due to temperature and latent heat associated with vapor pressure change for a small increment of soil. Terms on the right-hand side represent net thermal conduction into a small increment of soil, net thermal advection into an increment of soil due to water flux, and latent heat of evaporation in an increment of soil, respectively. Soil thermal conductivity and heat capacity are quantified using the theory of DeVries (1963). Heat advection by infiltration and redistribution is accounted for by considering the heat content of water flux into and out of a soil layer (RZWQM Team, 1992). The surface boundary condition is specified as a soil heat flux, G, which is obtained independent of Eq. [1] in a discrete surface energy balance model. Equation [1] can be discretized into a finite difference scheme and solved using a Newton–Raphson algorithm (Campbell, 1985).

Surface Boundary Conditions

A surface soil heat flux (G) boundary condition is obtained from PENFLUX that provides a solution to soil and residue energy balance equations. This surface boundary condition module uses a simplified soil heat flux equation and reduced forms of radiative and convective transfer schemes to simulate energy balance for a soil surface with incomplete residue cover and standing stems, providing an energy flux (G) boundary condition for Eq. [1]. The simplified soil heat flux is computed as the sum of gradient and storage terms for a soil slab of thickness Δz_s (Luo et al., 1992):

$$G = \frac{k_{t(s)}\,(T_{s(t)} - \hat{T}_{z(t)})}{\Delta z_s} - \frac{C_s(T_{s(t)} - T_{s(t-\Delta t)})}{2\Delta t} \quad [2]$$

To obtain $T_{s(t)}$, we must evaluate interacting effects of weather, residue architecture and soil conditions.

We use an electrical analog (Campbell, 1985, p. 2–5) to depict energy fluxes down thermal or vapor pressure gradients, opposed by transfer coefficients formulated as resistances. This gradient–diffusion, or K-theory, model proposes that the magnitude of energy flux is directly proportional to the driving gradient, and inversely proportional to a transport parameter formulated as a resistance. The analysis of Raupach (1987) indicates that K-theory is inadequate to describe exchange processes within vertically distributed evaporative sources, such as transpiring canopies. However, turbulent exchange for near-surface evaporative sources closely follows the far-field component of Lagrangian transport theory, which is adequately represented by the diffusion equation of K-theory (Raupach, 1989).

A diagrammatic representation of energy balance equations for soil and residue sublayers is given in Fig. 1. Convective transfer coefficients correspond to sensible and latent heat flux densities above the displacement plane associated with standing residue elements ($r_{a(a)}$, H, λE), within the residue layer ($r_{b(r)}$, $r_{s(r)}$, H_r, λE_r), and within the surface soil layer ($r_{h(r)}$, $r_{v(r)}$, $r_{s(s)}$, H_s, λE_s). Fluxes emanating from soil and residue surfaces are referenced to ambient conditions within the flat residue sublayer. Net irradiance at the residue ($R_{n(r)}$) and soil ($R_{n(s)}$) surfaces are important driving variables partitioned in a transmission scheme based on the principle of superposition (RZWQM Team, 1992). Ambient temperature and vapor pressure conditions are specified boundary conditions at the reference height ($T_{a(a)}$ and $e_{a(a)}$) and state conditions within the residue sublayer ($T_{a(r)}$ and $e_{a(r)}$). State conditions are also specified for the evaporative sources of surface residues (T_r and e_r) and the soil surface layer (T_s and e_s). Soil temperature is specified at the lower boundary of a soil slab, T_z. Soil heat flux, G, is a significant source–sink term computed from soil thermal gradients and time change, using soil thermal conductivity ($k_{t(s)}$) and heat capacity (C_s). Equations used to quantify these terms are detailed below.

Noting that the temperature of the evaporative surface is a common term in each element of the energy balance equation, we extend the Penman-type solution of McArthur (1990) to evaporative surfaces in soil and residue layers. We recognize an internal resistance ($r_{s(s)}$) opposing vapor, but not heat transport from the evaporative soil surface beneath the dust mulch to air within the residue layer. Resistance to heat ($r_{h(r)}$) and vapor ($r_{v(r)}$) transport from the surface soil to air in the midpoint of the flat residue layer is defined as a combination of molecular diffusivity and forced convection (Bristow et al., 1986; Tanner and Shen, 1990). Following Monteith (1973, p. 176), our application of the soil energy balance equation accommodates the ratio of vapor and heat resistances in the formulation of γ_s^*. For energy-limiting evaporation, we define γ_s^* as $\gamma(r_{s(s)} + r_{v(r)})/r_{h(r)}$ and compute surface soil source temperature, T_s, as

$$T_s = T_{a(r)} + \frac{r_{h(r)}}{C_a} \frac{\gamma_s^*}{(\Delta + \gamma_s^*)} (R_{n(s)} - G) - \frac{\delta e_{a(r)} - \delta e_s}{\Delta + \gamma_s^*} \quad [3a]$$

where the independent terms represent soil warming due to radiation absorbed under saturation water vapor pressures and soil cooling due to gradients in water vapor saturation deficits. The vapor pressure deficit term for the soil layer (δe_s) accounts for nonsaturating conditions for vapor in equilibrium with water at a characteristic water potential (Van Bavel and Hillel, 1976; see soil resistance, Eq. [10]), but can be neglected, as the relative humidity of vapor in equilibrium with soil water at 0.03 MPa tensions is about 99.98%, resulting in negligible vapor pressure deficits. When water flux to the evaporative surface limits evaporation, soil properties (rather than atmospheric demand) determine latent heat flux, invalidating assumptions required for the Penman-type solution. For supply-limiting evaporation, defined below, we compute surface soil temperature as

$$T_s = T_{a(r)} + \frac{r_{h(r)}}{C_a} (R_{n(s)} - G - \lambda E_s) \quad [3b]$$

obtaining estimates of λE_s from the soil-limiting supply of water to the evaporative surface, computed in antecedent solutions to the soil water balance. The transition from energy-limiting to supply-limiting evaporation is determined by the minimum of (i) potential evaporative demand, determined by

$$\lambda E_s = \frac{\Delta(R_{n(s)} - G) + C_a \frac{(\delta e_{a(r)} - \delta e_s)}{r_{v(r)}}}{\Delta + \gamma_s^*} \quad [4a]$$

or (ii) source evaporative supply, here obtained as the latent heat equivalent of water flux to the surface soil layer, plus potential loss of water storage in the surface soil layer. This is quantified from a previous time step from an associated water balance module, such as the RZWQM solution to the soil water balance (RZWQM Team, 1992). Alternatively, source evaporative supply can be calculated by

$$\lambda E_s = \frac{\lambda \rho_w \theta_v L}{\Delta t} \quad [4b]$$

where L can be defined as a depth sufficient to represent potential water loss (e.g., from a soil slab). When source evaporative supply exceeds evaporative demand, evaporation rate is energy-limited and surface temperature is computed by Eq. [3a]; else evaporation rate is supply-limited and surface temperature is computed by Eq. [3b].

We derive an analogous pair of equations for surface residue temperature, T_r, used to compute long-wave radiative exchanges, while also providing boundary condition information for residue water balance and decomposition modules. Defining γ_r^* as $\gamma(r_{s(r)} + r_{b(r)})/(r_{b(r)})$, we compute surface residue temperature for energy-limiting evaporation by

$$T_r = T_{a(r)} + \frac{r_{b(r)}}{C_a} \frac{\gamma_r^* R_{n(r)}}{(\Delta + \gamma_r^*)} - \frac{\delta e_{a(r)} - \delta e_r}{\Delta + \gamma_r^*} \quad [5a]$$

For supply-limiting evaporation, we compute residue source temperature as

$$T_r = T_{a(r)} + \frac{r_{b(r)}}{C_a} (R_{n(r)} - \lambda E_r) \quad [5b]$$

For simplification, we assume dry residue conditions in this study, taking residue evaporation as zero.

Ambient temperature ($T_{a(r)}$) and vapor pressure ($e_{a(r)}$) in the residue layer are computed as weighted averages of soil, residue, and ambient conditions. Equating sensible heat flux above the flat residue layer with the sum of fluxes from residue and soil sources, we solve for $T_{a(r)}$, obtaining weighting factors from resistance terms:

$$T_{a(r)} = \left(\frac{T_s}{r_{h(r)}} + \frac{T_r}{r_{b(r)}} + \frac{T_{a(a)}}{(r_{a(r)} + r_{a(a)})}\right) \left(\frac{1}{r_{h(r)}} + \frac{1}{r_{b(r)}} + \frac{1}{(r_{a(r)} + r_{a(a)})}\right)^{-1} \quad [6]$$

Using a similar approach for latent heat flux, and assuming zero residue evaporation, we solve for $e_{a(r)}$, and obtain weighting factors for vapor pressure within the residue layer:

$$e_{a(r)} = \left(\frac{e_s}{(r_{s(s)} + r_{v(r)})} + \frac{e_{a(a)}}{(r_{a(r)} + r_{a(a)})}\right) \left(\frac{1}{(r_{s(s)} + r_{v(r)})} + \frac{1}{(r_{a(r)} + r_{a(a)})}\right)^{-1} \quad [7]$$

Convective heat transfer coefficients are formulated as resistances, corresponding to regions bounded by specified temperature and vapor pressure conditions. Aerodynamic resistance between the zero displacement plane of standing residues and the height of ambient reference measurements is the integration of the eddy diffusion function within these limits (Choudhury and Monteith, 1988). Aerodynamic resist-

ances between the displacement plane and soil roughness length is quantified by integrating the eddy diffusion function between these limits. In the absence of standing residues, the displacement plane collapses to the soil surface, $r_{a(r)}$ goes to zero, and $r_{a(a)}$ can be approximated by the eddy diffusion function. Heat and vapor transport from the soil surface to the midpoint of the residue layer, assumed equivalent, are conceived as bulk aerodynamic resistances within the residue layer, $r_{h(r)}$ and $r_{v(r)}$. Their characteristic dimension is the distance from the soil surface to the midpoint of the flat residue layer, and they are computed as a function of wind speed at 10 mm above the flat residue layer:

$$r_{v(r)} = r_{h(r)} = \frac{z_{h(r)}}{2}\left[h_o(1 + s_c u_{zh(r)+10mm})\right]^{-1} \quad [8]$$

where h_o is molecular diffusivity of water vapor in still air. The linear form of the wind speed dependence of Eq. [8] is supported by data reported by Sauer and Norman (1995) from controlled heat and vapor sources within maize canopies. The convective scaling coefficient, s_c, is taken as 2, an intermediate value between similar scaling coefficients obtained for a 20-mm layer of wheat straw (Kimball and Lemon, 1971) and an 11-mm layer of flailed corn residue (Tanner and Shen, 1990). A boundary layer resistance to heat and vapor efflux from residue element surfaces to the midpoint of the residue sublayer, $r_{b(r)}$, is quantified as a power function of residue characteristic dimensions and near-surface wind velocity (Campbell, 1973, p. 67):

$$r_{b(r)} = 307\left(\frac{d_r}{u_{zh(r)+10mm}}\right)^{1/2} \quad [9]$$

A soil resistance, conceived as an impedance to vapor flux through a dry dust mulch for energy-limiting evaporation (Choudhury and Monteith, 1988), is quantified as

$$r_{s(s)} = \frac{l\tau}{h_o\theta_a} \quad [10]$$

where τ is soil tortuosity (here taken as 1.0) and l, the thickness of the dust mulch layer, is

$$l = L\left(1 - \frac{\theta_v}{\theta_\psi}\right) \quad [11]$$

with L equal to the depth of the surface soil layer (here taken as 10 mm), θ_v is average volumetric water content for the surface soil layer, and θ_ψ is volumetric soil water content at a characteristic water tension (here taken as 0.03 MPa). An internal resistance to vapor flux from residue elements, $r_{s(r)}$, is left undefined, as residue evaporation is assumed zero in this study.

Shortwave irradiance is partitioned to residue and soil layers by the principle of superposition, considering reflective properties (α_s, α_r) and fractional surface cover (A_r) for the flat residue layer:

$$R_{sn(s)} = (1 - \alpha_s)(1 - A_r)R_s \quad [12]$$

$$R_{sn(r)} = [(1 - \alpha_r) + \alpha_s(1 - A_r)]A_r R_s \quad [13]$$

This simplified formulation neglects the distinctions between beam and diffuse radiation and a residue transmission coefficient for diffuse radiation that are specified in Ross et al. (1985), Bristow et al. (1986), Flerchinger (1987), Hares and Novak (1992), and Bussiere and Cellier (1994), thus avoiding iterative numerical procedures. The Stefan–Boltzmann principle guides computation of longwave radiative exchange, considering temperatures, thermal emissivities, and superposition

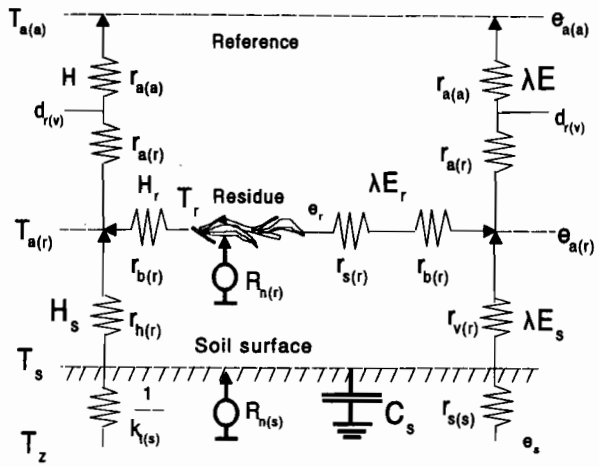

Fig. 1. An electric resistance analog of heat and vapor exchange in a soil–residue system as simulated by PENFLUX. For variables, see the Appendix.

of soil and residue layers:

$$R_{ln(s)} = (1 - A_r)R_{l(a)} + A_r R_{l(r)} - R_{l(s)} \quad [14]$$

$$R_{ln(r)} = (R_{l(a)} + R_{l(s)} - 2R_{l(r)})A_r \quad [15]$$

where $R_{l(i)} = \epsilon_i \sigma T_{iK}^4$ (with the subscript variable i standing for soil, residue, or atmospheric components). Net irradiance for soil and residue layers is the sum of shortwave and longwave components:

$$R_{n(s)} = R_{sn(s)} + R_{ln(s)} \quad [16]$$

$$R_{n(r)} = R_{sn(r)} + R_{ln(r)} \quad [17]$$

The saturated vapor pressure function and its derivative are computed from Campbell (1973, p. 22), as are humidities of soil and residue surfaces.

The coupled soil–residue energy balance equations (Eq. [3] and [5]) are combined with equations specifying ambient conditions in the residue sublayer (Eq. [6] and [7]), resistance terms (Eq. [8], [9], and [10]), radiation terms (Eq. [16] and [17]), and the reduced soil heat flux equation (Eq. [2]), and then solved for temperatures of soil and residue surfaces using Newton's method (Bristow, 1987). The soil slab lower boundary condition, $\hat{T}_{z(t)}$, is included in the iterative solution, adjusted by solving Eq. [2] for $\hat{T}_{z(t)}$ with interim G-values until the coupled soil–residue energy balance equations converge to 0.01°C. Soil heat flux, computed in Eq. [2], provides the surface flux boundary condition for Eq. [1]. The module is executed at hourly time steps, though daily time steps are feasible. This developmental version of RZWQM is written in FORTRAN, and required 15 min to simulate a 187-d period using hourly time steps on a 33-MHz 386 microcomputer

Field Experiments

We quantified soil and residue microclimatic conditions after the 1994 wheat (*Triticum aestivum* L. cv. TAM 107) harvest at the Colorado State University Horticultural Field Station located 5 km northeast of Fort Collins, CO (40°38′ N, 104°59′ W; 1530 m elevation). The study site was located on a level Nunn clay loam soil divided into 16 31.2- by 15.2-m management units containing either cropped or fallow phases of a wheat–fallow cropping system study. Flat and standing wheat residues distributed by the International Harvestore

1420 combine,[1] fitted with a 6.1-m header, were left undisturbed on management units that were previously under no-till management. Thus, residue distribution included standing and flat residues, as expected on commercial farms under no-till chemical fallow. After harvest on Day 209, data acquisition began on Day 213 and continued through Day 258 in 1994 for wheat stubble in a single management unit.

An automated data acquisition system (Campbell Scientific 21X data logger, Logan, UT) measured incident horizontal solar (LI-COR 200S, Lincoln, NE) and net irradiance (REBS Q*5.5, Seattle, WA), air temperature, and wind speed (Met-One 014A, Grants Pass, OR) at 2 m. Instruments were factory-calibrated at time of manufacture (1993) and verified at completion of the study. Data samples were collected once each minute and integrated into hourly values. Daily average vapor pressure was calculated from temperature and relative humidity (Campbell Scientific HMP35C) measured and computed each 3 s at the 2-m reference height and averaged over the 24-h period. Soil temperature sensors included sets of three thermocouples (0.51 mm diam., wired in parallel) placed 0.01, 0.025, 0.05, and 0.15 m below the soil surface. Air temperature was measured with 0.13-mm-diam. thermocouples located 0.03, 0.20, and 0.50 m above the soil surface. Three sets of bare 0.51-mm thermocouples, inserted axially within hollow residue stems, monitored residue temperatures at 0.03 m above the soil surface. All thermocouples were copper–constantan. Cup anemometers (Met-One 5758 and 014A), located 0.3 and 0.5 m above the soil surface, measured wind speeds at the center of each unit. Sensors were sampled once each minute and averaged at hourly intervals.

Surface residue cover (61%) was determined by a line-transect method, using 10 1-m transects. Dimensions of standing wheat stems (height = 0.3 m; frequency = 390 stems m^{-2}; diameter = 3 mm) were determined using ten 0.1-m samples of row (0.3-m row spacing). We estimated loss of residue mass (initially 7.0 Mg ha^{-1}), related to surface cover (Shaffer and Larson, 1987) using a first-order kinetic model of decomposition (Douglas and Rickman, 1992). Long-wave emissivity of soil and residue was specified as 0.96 (Salisbury and D'Aria, 1992). Atmospheric emissivity was defined as a function of ambient temperature (Idso and Jackson, 1969), modified by apparent cloud cover (Bristow et al., 1986). Flerchinger (1987) reported the albedo of wheat residue as 0.40, determined for 100% surface cover by flat wheat residues. Wind profile slope and surface roughness were determined from wind speed measurements above and within standing residues, relative to reference wind speed (Rosenberg et al., 1983, p. 139).

Soil physical properties were determined for soil horizons to a depth of 1.4 m at the experimental site. Measured surface horizon physical properties included bulk density (1.2 Mg m^{-3}), texture (f_{sand} = 0.25, f_{silt} = 0.33, f_{clay} = 0.42), and the water retention curve [$\psi_m = -0.25\ m\ (\theta_v/\theta_s)^{-6.37}$; Campbell, 1985, p. 43]. We inferred saturated hydraulic conductivity values for soil horizons (8.3×10^{-6} m s^{-1} for the surface horizon) from texture, bulk density, and organic matter (Ahuja et al., 1988). Initial soil water distribution was determined by neutron thermalization. Soil temperature was initialized at ambient conditions. Soil albedo, distinct from residue albedo, varied as a linear function of surface water content between wet (0.21) and dry (0.31) extremes, obtaining these reflectance values from a nonlinear function of the soil color attribute called *value*, determined by reference to a Munsell color chart (Fimbres et al., 1995). No calibration parameters were used to fit model calculations to measurements. Model parameters were obtained either by direct measurement or by reference to the literature.

[1] Mention of a trademark or proprietary product does not constitute a guarantee or warranty by the USDA and does not imply its approval over other products that may also be suitable.

Table 1. Mean daily weather conditions for evaluation of energy simulation within a soil–residue system (Ft. Collins, CO, 1994).

	Environmental conditions†				
Day of Year	R_s‡	R_n	$T_{a(a)}$	$e_{a(a)}$	u_a
	– MJ m^{-2} d^{-1} –		°C	kPa	m s^{-1}
227	27.3	16.0	20.8	1.39	3.22
229	27.2	15.4	22.0	1.38	1.73
230	13.8	6.7	20.9	1.36	2.83
231	14.1	7.8	17.5	1.31	1.63

† R_s, solar irradiance; R_n, net irradiance (for soil and flat residne layers); T_a, ambient temperature; e_a, ambient vapor pressure; u, wind speed. The T, e, and u variables are measured at a fixed reference height a. (See also Appendix.)

‡ Daily energy flux components reported as MJ m^{-2} d^{-1} can be converted to W m^{-2} (as used in the equations) with the multiplier 11.574.

Accuracy and Efficiency of Calculated Values

The accuracy and efficiency of hourly values calculated by PENFLUX are compared with field measurements. Predictive efficiency, a measure of predictive accuracy relative to variability inherent in the data, was quantified (Nash and Sutcliffe, 1970; Green and Stephenson, 1986) as

$$\text{Eff} = \left[1 - \frac{\sum (y - \bar{y})^2}{\sum (y - \bar{y})^2}\right] \times 100 \qquad [18]$$

We provide detailed analysis of accuracy and efficiency for Days 227, 229, 230 and 231, when surface residue and soil layers were dry and the principal weather variation was either in radiation or wind speed (Table 1). Overall bias and precision of model predictions were quantified by linear regression.

RESULTS

The model was initialized on Day 213 and run continuously for 45 d; limited rain occurred during the evaluation period. Model performance was evaluated for four days when soil and residue surfaces were dry, irradiance was moderate (Days 230, 231) or high (Days 227, 229), and mean daily wind speeds were low (Days 229, 231) to moderate (Days 227, 230) (Table 1). Day 228 was

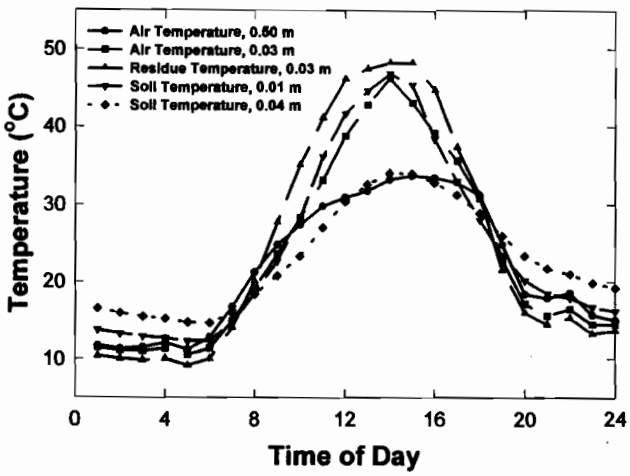

Fig. 2. Hourly fluctuations in soil–residue temperatures observed for wheat residues at 16 d after harvest.

Table 2. Accuracy and efficiency of calculated values of hourly net irradiance and residue, soil surface, and near-surface ambient temperatures on four evaluation days.

		Net irradiance, R_n				Residue temperature, T_r				Surface soil temperature, T_s				Near-surface ambient temperature, $T_{a(r)}$§			
DOY†	N‡	a_0	a_1	r^2	Eff	a_0	a_1	r^2	Eff	a_0	a_1	r^2	Eff	a_0	a_1	r^2	Eff
227	24	−35.2	1.012	0.991	97.4	3.69	0.889**	0.983	96.9	5.48*	0.789**	0.956	92.5	2.36	0.959*	0.970	95.5
229	24	−29.9	0.980	0.987	97.0	3.14	1.01	0.973	91.7	6.50*	0.798**	0.934	89.7	1.78	1.079	0.948	83.6
230	24	−26.4*	1.094**	0.994	96.5	1.68	1.022	0.994	95.2	5.95**	0.788**	0.960	90.5	0.08	1.104**	0.988	90.6
231	24	−36.4**	0.963*	0.995	93.9	1.36	1.025	0.986	94.7	4.54**	0.808**	0.964	93.1	−0.46	1.124**	0.978	89.9
Pooled	96	−31.2	0.998	0.988	96.8	2.59	0.978	0.974	94.7	5.43*	0.804**	0.947	91.6	1.12	1.055*	0.960	90.1

*,** Significant difference at the 0.05, 0.01 probability levels, respectively, testing H_0: $a_0 = 0$, $a_1 = 1$.
† DOY, Day of Year, 1994.
‡ N, number of observations; a_0, intercept; a_1, slope; r^2, coefficient of determination; Eff, % predictive efficiency.
§ Near-surface is defined as 0.03 m above the soil surface. (See also Appendix.)

omitted from the evaluation period because a 2-mm rainfall compromised the assumption of dry surface residues.

Hourly measurements of soil, residue, and air temperatures for Day 229, a day with high irradiance and low wind speeds, are shown in Fig. 2. This figure depicts daily temperature changes near the soil surface. Negative residue–soil thermal gradients at night are reversed with daytime heating by solar radiation. The similarity of near-surface air, soil, and flat residue temperatures demonstrates the close coupling of the near-surface thermal regime with partial residue cover, indicating potential application of infra-red thermometry. The cooler daytime temperatures of subsoil and reference air demonstrate the effects of aerodynamic resistance and soil thermal inertia on heat exchange from the soil surface. We evaluated the ability of the PENFLUX module to quantify the thermal dynamics of this soil–residue–atmosphere system.

Simulation results with PENFLUX are correlated with hourly measurements (Table 2), though systematic biases reduce predictive accuracy in some cases. Predictive efficiency is limited either by random error or by systematic bias. The high coefficient of determination ($r^2 > 0.93$ in all cases) indicates a low degree of random error (Table 2). Systematic bias, indicated by deviation of slope and intercept from unity and zero, respectively, provides evidence of conceptual or quantification error. (In the Discussion section, we identify likely sources of conceptual errors by inspection of the fundamental equations, and discuss research needs.)

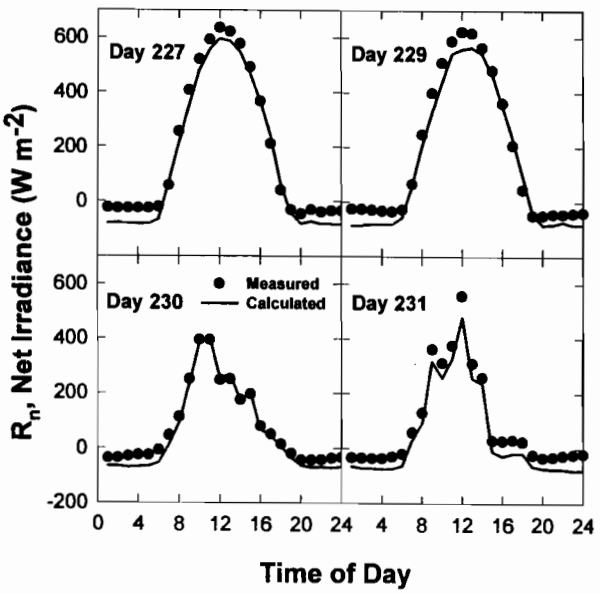

Fig. 3. Simulated and observed hourly fluctuations in net irradiance over a soil–residue system at 14, 16, 17, and 18 d after wheat harvest.

The timing of simulated R_n (Fig. 3) extremes is closely reproduced by PENFLUX calculations. Irradiance loading on Days 227 and 229 reflected that of generally clear skies, while intermittent cloud cover reduced insolation on Days 230 and 231. Net irradiance calculated by PENFLUX was generally lower than measurements—constituting a bias for Days 230 and 231, days with moderate irradiance. This trend could result from reflective properties of standing residues which are not explicitly considered in PENFLUX.

A negative bias persists in simulated nighttime net irradiance. This bias is partially attributable to a positive bias in soil temperature. For example, when a bare soil surface temperature of 15°C is overestimated by 5°C, the bias propagated to net irradiance via the simulation of thermal radiation emitted by the soil is −27 W m^{-2}. Thus, error propagated from biased soil temperatures contributes to nocturnal R_n bias. Since partial residue cover would reduce the magnitude of this bias, other factors, such as an underestimate of clear-sky atmospheric thermal emittance (ϵ_a) could contribute to systematic bias in the nocturnal radiation balance. However, the values for ϵ_a obtained as a function of ambient temperature (Idso and Jackson, 1969) are within the

Table 3. Energy balance partitioning simulated by energy balance for a soil–residue system.

	Energy balance components‡§						
DOY†	$R_{n(r)}$	$R_{n(s)}$	H_r	H_s	λE_s	$\lambda E_{s,G=0}$	G
	MJ m^{-2} d^{-1}						
227	6.23	6.88	6.22	−0.71	5.62	6.95	1.97
229	5.28	7.27	5.26	−1.23	6.00	7.78	2.50
230	2.13	2.90	2.13	−0.38	3.48	3.32	−0.17
231	2.12	2.19	2.14	0.85	2.58	1.77	−1.23

† DOY, Day of Year (1994).
‡ $R_{n(r)}$ and $R_{n(s)}$, net irradiance at the residue and soil surfaces; H_r and H_s, sensible heat flux density from residue and soil elements; λE_s, latent heat flux density from soil surface; $\lambda E_{s,G=0}$, lateut heat flux density from soil surface with G assumed zero; G, soil heat flux density. (See also Appendix.)
§ Energy balance compouents reported as MJ m^{-2} d^{-1} can be converted to W m^{-2} (as used in the equations) with the multiplier 11.574.

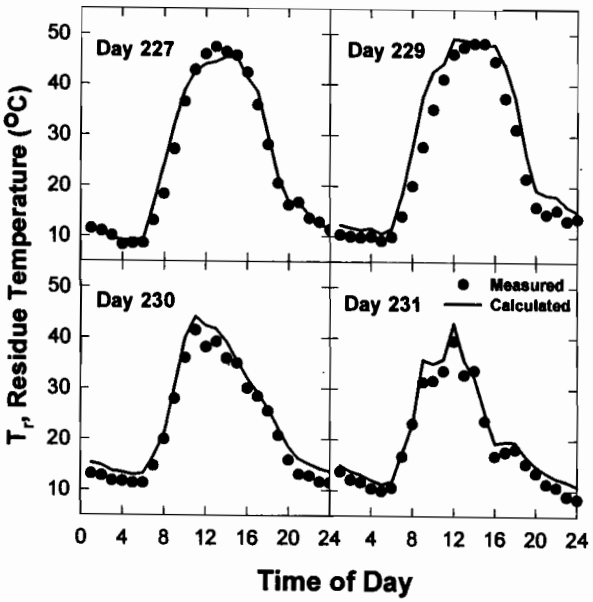

Fig. 4. Simulated and observed hourly fluctuations in surface wheat residue temperatures within a soil–residue system at 14, 16, 17, and 18 d after wheat harvest.

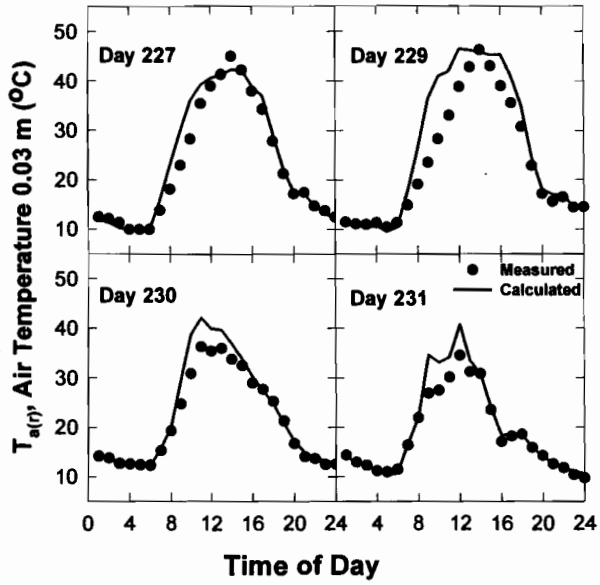

Fig. 6. Simulated and observed hourly fluctuations in near-surface ambient temperatures within a soil–residue system at 14, 16, 17, and 18 d after wheat harvest.

range of values obtained from ambient vapor pressure functions, determined to have zero bias under agricultural environments (Hatfield et al., 1983). Further, Flerchinger et al. (1996) found mean bias error for incoming long-wave radiation was lower than that of other radiation balance components for a snowpack. Sensor calibration error is not likely to account for calculated error, as the relatively small sensor signal observed at night would not propagate much bias in calibration coefficients.

Model calculations reproduce daily fluctuations measured in surface residue (Fig. 4), soil (Fig. 5) and near-surface air (Fig. 6) layers. Calculated T_s exhibits a systematic bias (Fig. 5), overestimating the nocturnal minima and underestimating the diurnal maxima for all four evaluation periods. The consistency of this bias, and its coincidence with irradiance loading, suggests that the bias results from errors in quantification of radiation partitioning either in quantification of residue cover or in representation of radiation transmission processes. Underestimates of radiation transmission through the residue layer could account for this bias, which appears proportional to irradiance but not to wind conditions. The apparent time lag in occurrence of calculated thermal maxima for T_s may relate to errors in radiation partitioning as well. The timing and magnitude of thermal maxima and minima are closely represented for T_r (Fig. 4) and $T_{a(r)}$ (Fig. 6), though calculation of $T_{a(r)}$ by PENFLUX resulted in a slight positive bias (Table 2). This bias could result from systematic error in calculation of radiative and/or convective exchange processes. Further comparison of model calculation with measurements under a variety of soil, residue, and weather conditions may isolate systematic errors in calculation of near-surface exchange processes.

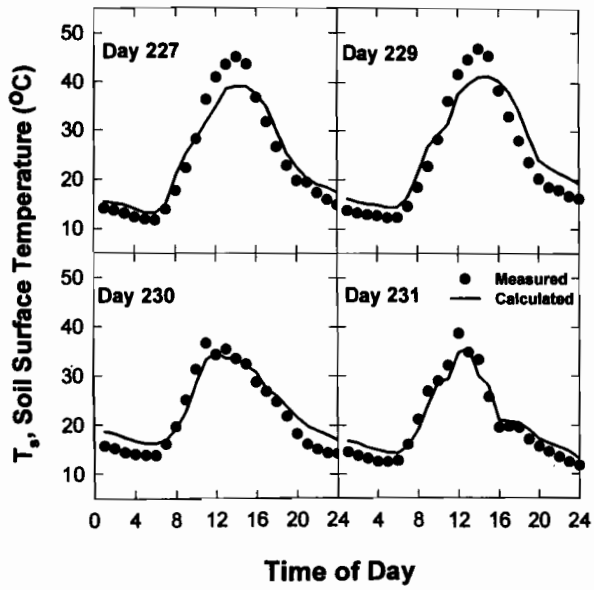

Fig. 5. Simulated and observed hourly fluctuations in surface soil temperatures within a soil–residue system at 14, 16, 17, and 18 d after wheat harvest.

Components of the soil–residue energy balance, calculated by PENFLUX, are presented in Table 3. The flat residue layer absorbed 42 to 49% of net irradiance in the soil–residue system, dispersing energy as sensible heat to atmosphere and soil layers, as calculated by PENFLUX. Simulated net irradiance at the soil surface was strongly partitioned to water evaporation and soil heat flux. This result is consistent with observation of small thermal gradients among near-surface layers (Fig. 2). Soil heat flux, as calculated by PENFLUX, accounted for −28.4 to 19.9% of net radiation absorbed by soil and residue layers, on a daily basis. We attribute the negative fraction obtained on Day 231 to soil heat loss resulting from cooler ambient conditions and reduced radiation relative to conditions of the preceding day.

Conversely, soil warming on Day 229 is associated with high radiation loading and warmer ambient conditions. The relative magnitude of soil heat as a sink for net radiation is of the same order reported by Allmaras et al. (1977) for bare soil, and within one standard deviation of the mean ratio obtained under senescent or vegetated shortgrass steppe with leaf area index (LAI) from 0 to 0.5 from April to October (Lapitan and Parton, 1996).

The storage component of soil heat flux (the second term on the right side of Eq. [2]) represents a dynamic feature of the surface energy balance system—quantifying effects of antecedent conditions on current energy transfer. Neglecting this dynamic feature can introduce bias to calculations of energy balance components.

The common assumption that daily soil heat flux is zero (RZWQM Team, 1992) can result in significant bias in calculation of daily evaporation of water. The magnitude of this bias is demonstrated in Table 3, where $\lambda E_{s,G=0}$ is obtained using Eq. [4a] and the assumption $G = 0$. On Day 229, a sunny day with soil warming, soil water evaporation would be overestimated by 30%; on Day 231, a cloudy day with soil cooling, a negative bias of −31% would result from the zero soil heat flux assumption. These biases are avoided in the PENFLUX energy balance algorithm by explicit specification of G.

DISCUSSION

The sensitivities of surface temperature to dynamic driving variables establishes this state condition as a significant test of surface energy balance models (Mahrer, 1979; Sui et al., 1992; Hares and Novak, 1992; Bussiere and Cellier, 1994; Grant et al., 1995). The linkage of surface temperatures and evaporative flux is well established (Fuchs and Tanner, 1967; Monteith, 1981), as the vapor pressure in equilibrium with water held in evaporative sources is an exponential function of surface temperature; following gradient–diffusion theory, evaporative flux increases exponentially with the temperature of the evaporative surface, all other conditions held constant. This sensitivity is expected to increase with surface dryness as what may be considered the buffering effect of the latent heat of evaporation diminishes. By inspection, when supply-limiting conditions hold (λE_s calculated by Eq. [4b] is less than that calculated by Eq. [4a]), T_s is greater when calculated by Eq. [3b] rather than Eq. [3a], illustrating the linkage of thermal and flux conditions for evaporative surfaces. Thus, accurate specification of the temperature of evaporative surfaces is a reasonable indication of predictive accuracy for noncalibrated surface energy balance models.

Shifts in surface temperature can correspond with significant shifts in energy balance partitioning. Van Duin (1956) demonstrated the sensitivities of surface temperature and energy balance components to the aerodynamic roughness parameter, z_o. This analysis shows that the annual amplitude of T_s would shift from 11 to 7°C when z_o increased from 1 to 20 mm, indicating that energy dissipation can shift from radiative and conductive processes to convective processes. This calculation is verified by Allmaras et al. (1977) using Bowen ratio techniques to quantify energy balance components of smooth and rough soil surfaces. They found that the rough surface averaged 6°C cooler than the smooth surface (from 0700 to 1920 h) and that the convective dispersion of energy ($H + \lambda E$) was 27% greater for the rough surface relative to the smooth surface. These results confirm Van Duin's calculation, demonstrate the linkage of surface temperature to near-surface exchange processes, and illustrate the significance of near-surface processes in shifting energy dispersion from radiative and conductive processes to convective processes.

The conceptual design of PENFLUX exploits the discontinuity of thermal properties at the soil–atmosphere interface to obtain simplification and predictive accuracy. The heat storage capacity of soil can be 10^3 times greater than that of air (Campbell, 1985, p. 32); while heat transfer by convection can be 10^2 times greater than transfer by conduction in dry soil (Nobel, 1983, p. 373, 473). The greater thermal inertia of soil and greater heat transport potential of convection suggests that soil surface temperature may be more sensitive to fluctuations in atmospheric boundary conditions relative to subsoil conditions over short time intervals. The representation of soil heat flux by a soil slab (Eq. [2]) builds on the conjecture that accurate solutions for surface temperatures may be less sensitive to uncertainties in subsoil temperatures than to uncertainties in radiative and convective exchange processes. This conjecture distinguishes PENFLUX from integrated numerical solutions to the surface energy balance equation, which use equations similar to Eq. [1] to quantify soil thermal processes. The formulation of $r_{v(r)}$ and $r_{s(s)}$ are necessary complements to the soil slab approximation of G, as quantification of near-surface resistances to sensible and latent heat flux is necessary to retain predictive accuracy. Determining the accuracy of surface temperature calculations provides a useful and convenient performance measure for evaluations of near-surface resistance formulations.

The formulation of $r_{s(s)}$ (Eq. [10]) transforms information regarding soil water supply to information regarding surface vapor flux—extending the applicability of the Penman equation beyond saturating conditions. This transformation promotes numerical efficiency by avoiding accurate specification of surface humidity. Accurate calculation of surface humidity would require sufficient spatiotemporal resolution in a numerical solution to the soil water balance equation to quantify the development of dust mulches during second-stage evaporation. An analogous transformation is required to quantify $r_{s(r)}$, resistance to vapor flux within residue elements. Also, an equation analogous to Eq. [4b] is required to evaluate the transition from energy-limiting to supply-limiting evaporation for the residue layer. The surface resistance and supply-limiting evaporation boundary conditions for the residue layer are probably necessary for accurate prediction of the thermal state of residue elements under evaporative conditions.

The PENFLUX solution to the surface energy balance equation is derived from gradient–diffusion theory—theory that is contradicted by observations of

counter-gradient flux in forest canopies (Denmead and Bradley, 1985). As Dolman and Wallace (1991, p. 1325–1326) wrote, "Generally, K-theory requires the characteristic length scale of the dominant eddies to be small compared with the distance over which the gradient changes appreciably. This is violated within most plant canopies where the length scale of the turbulence is of the same order as the canopy height." Resolving this conceptual defect, Raupach (1989) derived a Lagrangian method to distinguish near-field and far-field effects of turbulence on latent and sensible heat exchange within vegetative canopies. Application of this method to a dual-source evaporation model resulted in similar predictive accuracy as dual-source models derived with K-theory (Dolman and Wallace, 1991). K-theory quantification of turbulent transfer, assumed equivalent to the far-field component of the Lagrangian model, appears to be an adequate representation of near-surface convective exchange processes because near-surface turbulence becomes strongly inhomogeneous and the characteristic time scale approaches zero (Raupach, 1989). The characterization of near-surface transfer coefficients as a linear empirical function of wind speed Eq. [9] appears adequate to simulate surface thermal dynamics. However, conceptual advances in describing these processes may provide alternatives that reduce the degree of empiricism and ambiguity inherent in K-theory (e.g., parameterizing $d_{r(v)}$ and z_o) (McInnes et al., 1991).

Simplifications and novel features introduced by the PENFLUX module reduce numerical requirements for solution of the surface boundary condition equation. Three simplifications reduce numerical requirements for iteration:

1. Surface heat flux into the soil is approximated as heat stored and conducted in a soil slab, a truncation of the soil thermal profile quantified in more complex soil heat modules.
2. Radiation transmission is simulated by the principle of superposition, partitioning intercepted radiation in proportion to surface area cover, reflective and emittive properties, while neglecting the differences in sun angle and beam and diffuse radiation that are considered in more complex simulations (Ross et al., 1985; Bristow et al., 1986; Flerchinger and Saxton, 1989; Hares and Novak, 1992; Bussiere and Cellier, 1994).
3. A stability correction factor frequently used in convective transport algorithms (Choudhury and Monteith, 1988; Flerchinger and Saxton, 1989) is neglected in the RZWQM aerodynamic resistance formulations (RZWQM Team, 1992) applied to the PENFLUX module, further reducing iterative requirements.

Novel features introduced in PENFLUX involve referencing soil and residue surface temperature to near-surface air temperature, using resistances as weighting terms for $T_{a(r)}$, and specifying limits to the formulation of soil resistance to vapor flux. Both features accentuate effects of near-surface heat transfer coefficients and contribute to the accuracy of calculated values obtained with PENFLUX.

Despite simplifications that reduce numerical requirements for iteration, the PENFLUX solution to the surface energy balance equation was accurate for surface temperatures and net irradiance. The structure of PENFLUX permits quantification of water evaporation from a flat residue layer. However, a complementary residue water balance is required to provide surface resistance and supply limiting evaporation boundary conditions. When coupled with a residue water balance model, PENFLUX would be suitable for evaluating energy balance effects of dynamic residue architectures that result from microbial decomposition and structural redistribution processes. Simplified solutions to the surface energy balance equations, such as PENFLUX, offer numerically efficient boundary conditions to soil heat and water balance modules, as well as to models of biological processes that require limited information of soil. The process-level solution to the energy balance equation permits quantification of uncertainty propagated by the algorithm, and can support identification of critical scaling factors required for accurate simulation of energy exchange in a heterogenous landscape (Wagner, 1994).

CONCLUSIONS

PENFLUX, a simplified yet physically based boundary condition solution for soil–residue energy exchange, exhibited high predictive accuracy and efficiency for surface temperatures and net irradiance for standing and flat wheat residues under dry conditions, as implemented within RZ–SHAW. PENFLUX parameterization requirements are readily met by standard soil physical methods and straightforward characterization of residue cover and standing stem frequency. The conceptual design of PENFLUX exploits the discontinuity of thermal and transport properties at the soil–atmosphere interface, achieving simplification of subsoil boundary conditions while using near-surface resistance terms to retain sensitivity to soil–atmosphere boundary conditions. A positive bias in nighttime surface soil temperature is propagated to negative bias in nocturnal net radiation. Energy balance calculations by PENFLUX indicate that the common assumption of zero daily soil heat flux can result in a bias of ±30% in calculated evaporative demand. The predictive accuracy, reduced numerical requirements, and potential application of PENFLUX to soil heat and water models warrant further evaluation against measured data for a range of residue architectures and comparison with integrated soil–residue heat flow models. Subject to these evaluations, PENFLUX is applicable to a variety of land management problems that depend on accurate predictions of surface temperatures and energy flux components.

APPENDIX

The following are variables used in the text and equations (and in tables and figures), with their definitions and units. Bracketed numbers at the end of definitions indicate the equations in which the variables are used.

A_r Fractional area surface cover by flat residue, $m^2\ m^{-2}$ [12, 13, 14, 15]

C_a Volumetric heat capacity of air, $J\ m^{-3}\ K^{-1}$ [3a, 3b, 4a, 5a, 5b]

C_s Volumetric heat capacity of soil, J m^{-3} K^{-1} [1, 2]
C_w Volumetric heat capacity of water, J m^{-3} K^{-1} [1]
d_r Characteristic diameter of flat residue element, m [9]
$d_{r(v)}$ Zero displacement plane for vertical residue elements, m
$e_{a(a)}$ Ambient vapor pressure at reference height a, Pa [7]
$e_{a(r)}$ Ambient vapor pressure at midpoint of flat residue layer, Pa [7]
e_r Surface residue evaporative source vapor pressure, Pa
e_s Surface soil evaporative source vapor pressure, Pa [1, 7]
G Soil heat flux density, W m^{-2} [2, 3a, 3b, 4a]
h_o Molecular diffusivity of water vapor in still air, m^2 s^{-1} [8, 10]
H Sensible heat flux density above residue layer, W m^{-2}
H_r Sensible heat flux density from residue layer, W m^{-2}
H_s Sensible heat flux density from surface soil layer, W m^{-2}
$k_{t(s)}$ Thermal conductivity of soil, J m^{-1} K^{-1} s^{-1} [1, 2]
l Thickness of dust mulch layer, m [10, 11]
L Depth of surface soil layer, m [4b, 11]
M_w Molecular weight of water, kg mol^{-1} [1]
q_v Soil water vapor flux, kg m^{-2} s^{-1} [1]
q_w Soil water flux, m s^{-1} [1]
$r_{a(a)}$ Aerodynamic resistance to reference height a, s m^{-1} [6, 7]
$r_{a(r)}$ Aerodynamic resistance below zero displacement plane, s m^{-1} [6, 7]
$r_{b(r)}$ Boundary layer resistance within flat residue layer, s m^{-1} [5a, 5b, 6, 9]
$r_{h(r)}$ Thermal convective resistance within residue layer, s m^{-1} [3a, 3b, 6, 8]
$r_{s(r)}$ Residue element internal resistance to vapor flux, s m^{-1}
$r_{s(s)}$ Soil dust mulch internal resistance to vapor flux, s m^{-1} [7, 10]
$r_{v(r)}$ Vapor convective resistance within residue layer, s m^{-1} [4a, 7, 8]
R Universal gas constant, J K^{-1} mol^{-1} [1]
$R_{l(a)}$ Longwave irradiance emitted by atmosphere, W m^{-2} [14, 15]
$R_{l(i)}$ Longwave irradiance emitted by atmosphere, residue, or soil, W m^{-2}
$R_{l(r)}$ Longwave irradiance emitted by flat residue layer, W m^{-2} [14, 15]
$R_{l(s)}$ Longwave irradiance emitted by surface soil, W m^{-2} [14, 15]
$R_{ln(r)}$ Net longwave irradiance for flat residue layer, W m^{-2} [15, 17]
$R_{ln(s)}$ Net longwave irradiance for soil layer, W m^{-2} [14, 16]
R_n Net irradiance for soil and flat residue layers, W m^{-2}
$R_{n(r)}$ Net irradiance for flat residue layer, W m^{-2} [5a, 5b, 17]
$R_{n(s)}$ Net irradiance at soil surface, W m^{-2} [3a, 3b, 4a, 16]
R_s Solar irradiance on horizontal surface, W m^{-2} [12, 13]
$R_{sn(r)}$ Net shortwave irradiance for flat residue layer, W m^{-2} [13, 17]
$R_{sn(s)}$ Net shortwave irradiance for surface soil layer, W m^{-2} [12, 16]
s_c Scaling coefficient for residue convective resistance, s m^{-1} [8]
t Time, s [1]
Δt Time increment, s [2, 4b]
$T_{a(a)}$ Ambient temperature at reference height a, °C [6]
$T_{a(r)}$ Ambient temperature at midpoint of flat residue layer, °C [3a, 3b, 5a, 5b, 6]
T_{iK} Temperature of atmosphere (T_{aK}), residue (T_{rK}), or surface soil (T_{sK}), °K
T_r Residue temperature, °C [5a, 5b, 6]
T_s Surface soil temperature, °C [3a, 3b, 6]
$T_{s(t)}$ Surface soil temperature at time t, °C [2]
$T_{s(t-\Delta t)}$ Previous surface soil temperature, °C [2]
T_z Soil temperature at depth z, °C [1]
T_{zK} Soil temperature at depth z, °K [1]
$\hat{T}_{z(t)}$ Soil temperature expected at soil slab lower boundary z at time t, °C [2]
u_a Wind speed at reference height a, m s^{-1}
$u_{zh(r)+10mm}$ Wind speed at 10 mm above flat residue layer, m s^{-1} [8, 9]
y Observed value of parameter y [18]
$\bar{y}$ Mean value of parameter y [18]
$\tilde{y}$ Predicted value of parameter y [18]
z Vertical distance from soil surface, m [1]
z_o Aerodynamic roughness length, m
$z_{h(r)}$ Height of flat residue layer, m [8]
Δz_s Depth increment of soil slab, m [2]
α_r Shortwave reflectivity of residue layer [13]
α_s Shortwave reflectivity of surface soil [12, 13]
γ Psychrometric constant, Pa °C^{-1}
γ_r* Psychrometric constant, adjusted for residue internal resistance, Pa °C^{-1} [5a]
γ_s* Psychrometric constant, adjusted for soil internal resistance, Pa °C^{-1} [3a, 4a]
$\delta e_{a(r)}$ Ambient saturation deficit at midpoint of flat residue layer, Pa [3a, 4a, 5a]
δe_r Saturation deficit for residue, Pa [5a]
δe_s Saturation deficit for surface soil, Pa [3a, 4a]
Δ Slope of saturated vapor pressure function, evaluated at $T_{a(r)}$, Pa °C^{-1} [3a, 4a, 5a]
ϵ_i Longwave emissivity of soil (ϵ_s), residue (ϵ_r), or atmosphere (ϵ_a)
θ_a Volumetric air content in soil layer, m^3 m^{-3} [10]
θ_s Volumetric saturated water content in soil layer, m^3 m^{-3}
θ_v Volumetric water content in soil layer, m^3 m^{-3} [4b, 11]
θ_ψ Volumetric soil water content at characteristic tension, m^3 m^{-3} [11]
λ Latent heat of vaporization for water, J kg^{-1} [1, 4b]
λE Latent heat flux density above residue layer, W m^{-2}
λE_r Latent heat flux density from residue layer, W m^{-2} [5b]
λE_s Latent heat flux density from surface soil layer, W m^{-2} [3b, 4a, 4b]
$\lambda E_{s,G=0}$ Latent heat flux density from soil surface with G assumed zero, W m^{-2}
ρ_w Density of water, kg m^{-3} [4b]
σ Stefan–Boltzmann constant, J m^{-2} s^{-1} K^{-4}
τ Soil tortuosity for molecular diffusion [10]
ψ_m Soil water tension, m

Subscript Conventions

Subscripts are generally consistent across variables, particularly with r, s, w, and a used to indicate residue, soil, water, and air or atmosphere components. Occasionally the same letter subscript may carry different meanings in different contexts, as with the letter 'a', which may represent ambient (e.g., with temperature), aerodynamic (resistance), or (in italics) a fixed reference height, in addition to the use already mentioned (atmosphere). Where variables are further limited in terms of residue, soil, water, and atmosphere, these additional modifiers r, s, w, and a are put in parentheses (e.g., R_n for net irradiance, and $R_{n(s)}$ for net irradiance at the soil surface).

REFERENCES

Ahuja, L.R., J.W. Naney, R.D. Williams, and J.D. Ross. 1988. Vertical variability of soil properties in a small watershed. J. Hydrol. 99:307–318

Allmaras, R.R., E.A. Hallauer, W.W. Nelson, and S.D. Evans. 1977. Surface energy balance and soil thermal property modifications by tillage-induced soil structure. Minn. Agric. Exp. Stn. Tech. Bull. 306.

Bristow, K.L., G.S. Campbell, R.I. Papendick, and L.F. Elliott. 1986. Simulation of heat and moisture transfer through a surface-residue soil system. Agric. For. Meteorol. 36:193–214.

Bristow, K.L. 1987. On solving the surface energy balance equation for surface temperature. Agric. For. Meteorol. 39:49–54.

Bristow, K.L., and D.G. Abrecht. 1989. The physical environment of two semi-arid tropical soils with partial surface mulch cover. Aust. J. Soil Res. 27:577–587.

Bussiere, F., and P. Cellier. 1994. Modification of the soil temperature and water content regimes by a crop residue mulch: Experiment and modelling. Agric. For. Meteorol. 68:1–28.

Campbell, G.S. 1973. An introduction to environmental biophysics. Springer-Verlag, New York.

Campbell, G.S. 1985. Soil physics with BASIC: Transport models for soil–plant systems. Elsevier Sci. Publ. Co., Amsterdam.

Choudhury, B.J., and J.L. Monteith. 1988. A four-layer model for the heat budget of homogeneous land surfaces. Q. J. R. Meteorol. Soc. 114:373–398.

Chung, S-O., and R. Horton. 1987. Soil heat and water flow with a partial surface mulch. Water Resour. Res. 23:2175–2186.

Denmead, O.T., and E.F. Bradley. 1985. Flux–gradient relationships in a forest canopy. p. 421–442. *In* B.A. Hutchison and B.B. Hicks (ed.) The forest–atmosphere interaction. D. Reidel Publ. Co., Dordrecht.

DeVries, D.A. 1963. Thermal properties of soils. p. 210–235. *In* Physics of plant environment. W.R. Van Wijk (ed.) North-Holland Publishing Co. Amsterdam.

Dolman, A.J., and J.S. Wallace. 1991. Lagrangian and K-theory approaches in modelling evaporation from sparse canopies. Q. J. R. Meteorol. Soc. 117:1325–1340.

Doran, J.W., W.W. Wilhelm, and J.F. Power. 1984. Crop residue removal and soil productivity with no-till corn, sorghum and soybean. Soil Sci. Soc. Am. J. 48:640–645.

Douglas, C.L., and R.W. Rickman. 1992. Estimating crop residue decomposition from air temperature, initial nitrogen content, and residue placement. Soil Sci. Soc. Am. J. 56:272–278.

Fimbres, A., D.F. Post, A.D. Matthias, E.E. Sano, and A.K. Batchily. 1995. Soil albedo in relation to soil color and moisture. p. 296. *In* Agronomy abstracts. ASA, Madison, WI.

Flerchinger, G.N. 1987. Simultaneous heat and water model of a snow–residue–soil system. Ph.D. diss. Washington State Univ., Pullman (Diss. Abstr. 8813071).

Flerchinger, G.N., and K.E. Saxton. 1989. Simultaneous heat and water model of a freezing snow–residue–soil system: I. Theory and development. Trans. ASAE 32:565–571.

Flerchinger, G.N., J.M. Baker, and E.J.A. Spaans. 1996. A test of the radiative energy balance of the SHAW model for snowcover. Hydrol. Proc. 10:1359–1367.

Fuchs, M., and C.B. Tanner. 1967. Evaporation from a drying soil. J. Appl. Meteorol. 6:852–857.

Grant, R.F., R.C. Izaurralde, and D.S. Canasyk. 1995. Soil temperature under different surface managements: Testing a simulation model. Agric. For. Meteorol. 73:89–113.

Green, I.R.A., and D. Stephenson. 1986. Criteria for comparison of single event models. Hydrol. Sci. J. 31:395–411.

Gupta, S.C., W.E. Larson, and R.R. Allmaras. 1984. Predicting soil temperature and soil heat flux under different tillage–surface residue conditions. Soil Sci. Soc. Am. J. 48:223–232.

Hares, M.A., and M.D. Novak. 1992. Simulation of surface energy balance and soil temperature under strip tillage: I. Model description. Soil Sci. Soc. Am. J. 56:22–29.

Hatfield, J.L., R.J. Reginato, and S.B. Idso. 1983. Comparison of longwave radiation calculation methods over the United States. Water Resour. Res. 19:285–288.

Hillel, D., C.H.M. van Bavel, and H. Talpaz. 1975. Dynamic simulation of water storage in fallow soil as affected by mulch of hydrophobic aggregates. Soil Sci. Soc. Am. Proc. 39:826–833.

Idso, S.B., and R.D. Jackson. 1969. Thermal radiation from the atmosphere. J. Geophys. Res. 74:5397–5403.

Kimball, B.A., and E.R. Lemon. 1971. Air turbulence effects upon soil gas exchange. Soil Sci. Soc. Am. Proc. 35:16–21.

Lapitan, R.L., and W.J. Parton. 1996. Seasonal variabilities in the distribution of the microclimatic factors and evapotranspiration in a shortgrass steppe. Agric. For. Meteorol. 79:113–130.

Lascano, R.J., and C.H.M. van Bavel. 1983. Experimental verification of a model to predict soil moisture and temperature profiles. Soil Sci. Soc. Am. J. 47:441–448.

Lascano, R.J., R.L. Baumhardt, S.K. Hicks, and J.L. Heilman. 1994. Soil and plant water evaporation from strip-tilled cotton: Measurement and simulation. Agron. J. 86:987–994.

Luo, Y., R.S. Loomis, and T.C. Hsiao. 1992. Simulation of soil temperature in crops. Agric. For. Meteorol. 61:23–38.

Lyles, L., and B.E. Allison. 1976. Wind erosion: The protective role of simulated standing stubble. Trans. ASAE 19:62–64.

Mahrer, Y. 1979. Prediction of soil temperatures of a soil mulch with transparent polyethylene. Am. Meteorol. Soc. 18:1263–1267.

McArthur, A.J. 1990. An accurate solution to the Penman equation. Agric. For. Meteorol. 51:87–92.

McInnes, K.J., J.L. Heilman, and R.W. Gesch. 1991. Momentum roughness and zero-plane displacement of ridge-furrow tilled soil. Agric. For. Meteorol. 55:167–179.

Monteith, J.L. 1973. Principles of environmental physics. Edward Arnold. London.

Monteith, J.L. 1981. Evaporation and surface temperature. Q. J. R. Meteorol. Soc. 107:1–27.

Nash, J.E., and J.V. Sutcliffe. 1970. River flow forecasting through conceptual models: I. A discussion of principles. J. Hydrol. 44:282–290.

Nielsen, D., and S.E. Hinkle. 1994. Wind velocity, snow and soil water measurements in sunflower residues. Great Plains Agric. Council Bull. 150:93–100.

Nobel, P.S. 1983. Biophysical plant physiology and ecology. W.H. Freeman & Co., New York.

Norman, J.M., and P.G. Jarvis. 1975. Photosynthesis in sitka spruce (*Picea sitchensis* (Bong) Carr.): V. Radiation penetration theory and a test case. J. Appl. Ecol. 12:839–878.

Raupach, M.R. 1987. A Lagrangian analysis of scalar transfer in vegetation canopies. Q. J. R. Meteorol. Soc. 113:107–120.

Raupach, M.R. 1989. A practical Lagrangian method for relating scalar concentrations to source distributions in vegetation canopies. Q. J. R. Meteorol. Soc. 115:609–632.

Raupach, M.R. 1992. Drag and drag partition on rough surfaces. Boundary-Layer Meteorol. 60:375–395.

Rosenberg, N.J., B.L. Blad, and S.B. Verma. 1983. Microclimate: The biological environment. Wiley-Interscience, New York.

Ross, P.J., J. Williams, and R.L. McCowan. 1985. Soil temperature and the energy balance of vegetative mulch in the semi-arid tropics: I. Static analysis of the radiation balance. Aust. J. Soil Res. 23:493–514.

RZWQM Team. 1992. Root Zone Water Quality Model. Version 1.0. Technical documentation. USDA-ARS Great Plains Systems Res. Unit, Fort Collins, CO.

Salisbury, J.W., and D.M. D'Aria. 1992. Infrared (8–14 μm) remote sensing of soil particle size. Remote Sens. Environ. 42:157–165.

Sauer, T.J., and J.M. Norman. 1995. Simulated canopy microclimate using estimated below-canopy soil surface transfer coefficients. Agric. For. Meteorol. 75:135–160.

Shaffer, M.J., and W.E. Larson. 1987. NTRM, a soil–crop simulation model for nitrogen, tillage and crop-residue management. USDA-ARS Conserv. Res. Rep. 34-1.

Shuttleworth, W.J., and J.S. Wallace. 1985. Evaporation from sparse crops: An energy combination theory. Q. J. R. Meteorol. Soc. 111:839–855.

Stannard, D.I. 1993. Comparison of Penman–Monteith, Shuttleworth–Wallace and modified Priestley–Taylor evapotranspiration models for wildland vegetation in semiarid rangeland. Water Resour. Res. 29:1379–1392.

Sui, H-J., D-C. Zeng, and F-Z. Chen. 1992. A numerical model for

simulating the temperature and moisture regimes of soil under various mulches. Agric. For. Meteorol. 61:281–299.

Tanner, C.B., and Y. Shen. 1990. Water vapor transport through a flail-chopped corn residue. Soil Sci. Soc. Am. J. 54:945–951.

Van Bavel, C.H.M., and D.I. Hillel. 1976. Calculating potential and actual evaporation from bare soil surface by simulation of concurrent flow of water and heat. Agric. Meteorol. 17:453–476.

Van Doren, D.M., Jr., and R.R. Allmaras. 1978. Effect of residue management practices on the soil physical environment, microclimate, and plant growth. p. 49–83. *In* W.R. Oschwald (ed.) Crop residue management systems. ASA Spec. Publ. 31. ASA, CSSA, and SSSA, Madison, WI.

Van Duin, R.H.A. 1956. On the influence of tillage on conduction of heat, diffusion of air and infiltration of water in soil. Reports of Agric. Invest. No. 62.7 Netherlands Ministr. of Agric., Fisheries & Food Supply, The Hague.

Wagner, D.G. 1994. Determination of consumptive water use by remote sensing and GIS techniques for river basins. Ph.D. diss. Colorado State Univ., Fort Collins (Diss. Abstr. 9433279).